

Computational Methods for 3-D and Supersonic Flows

Helen L. Reed

Texas A&M University
Aerospace Engineering, 602B H.R. Bright Building, 3141 TAMU
College Station, Texas 77843-3141 USA

helen.reed@tamu.edu

3-D BOUNDARY-LAYER FLOWS

1.0 CROSSFLOW INSTABILITY

This section addresses the crossflow instability that causes the breakdown to turbulence in 3-D boundary layers that are characteristic of swept-wing flows. The papers of Reed & Saric (1989), Kohama et al. (1991), Kachanov (1996), Arnal (1997), Bippes (1997), Saric et al. (2003), Saric et al. (2004), Saric et al. (2008), Reed & Saric (2008), and Carpenter et al. (2009) provide an extensive list of references for recent experiments, including the DLR experiments in Germany on a swept flat plate, a Russian swept-flat-plate experiment, the CERT/ONERA experiments on swept wings, the Institute of Fluid Science work in Sendai on cones and spheres, the Arizona State University (ASU) swept-wing experiments, and the Texas A&M flight experiments. These papers established the existence of both travelling and stationary crossflow vortices, saturation of the stationary crossflow vortex, the nonlinear secondary instability leading to transition, and the sensitivity to freestream disturbances and surface roughness. Here are some great challenges to the computationalist.

One of the key missing ingredients in all 3-D boundary-layer experiments is the understanding of receptivity. Receptivity has many different paths through which to introduce a disturbance into the boundary layer and this “road map” is more complicated because of the amplified stationary vortices. In fact, many aspects of transition in 3-D boundary layers are orthogonal to 2-D boundary layers so such a “road map” is either not unique or too complicated. Aside from the usual mechanisms, such as the interaction of freestream turbulence and acoustical disturbances with model vibrations, leading-edge curvature, attachment-line contamination, discontinuities in surface curvature, etc., the presence of roughness that may enhance a stationary streamwise vortex is very important. In contrast to 2-D boundary layers where small 2-D roughness is important and 3-D roughness is less important unless it is large, the 3-D boundary layer appears to be ultra sensitive to micron-sized 3-D roughness within a small neighborhood of the leading edge. In this case, 2-D roughness is only important at its edges.

For swept wings, the crossflow instability occurs in the regions of strong pressure gradient, primarily near the attachment line. In the inviscid region outside the boundary layer, the combined influences of sweep and pressure gradient produce curved streamlines at the boundary-layer edge. Inside the boundary layer, the streamwise velocity is reduced but the pressure gradient is unchanged. Thus, the balance between centripetal acceleration and pressure gradient does not exist. This imbalance results in a secondary flow in the boundary layer called crossflow that is perpendicular to the direction of the local inviscid streamline. Because the crossflow velocity must vanish at the wall and at the boundary-layer edge, an inflection point exists and provides a

source of an inviscid instability mechanism. The 3-D profile and resolved streamwise and crossflow boundary-layer profiles are shown in Figure 1.

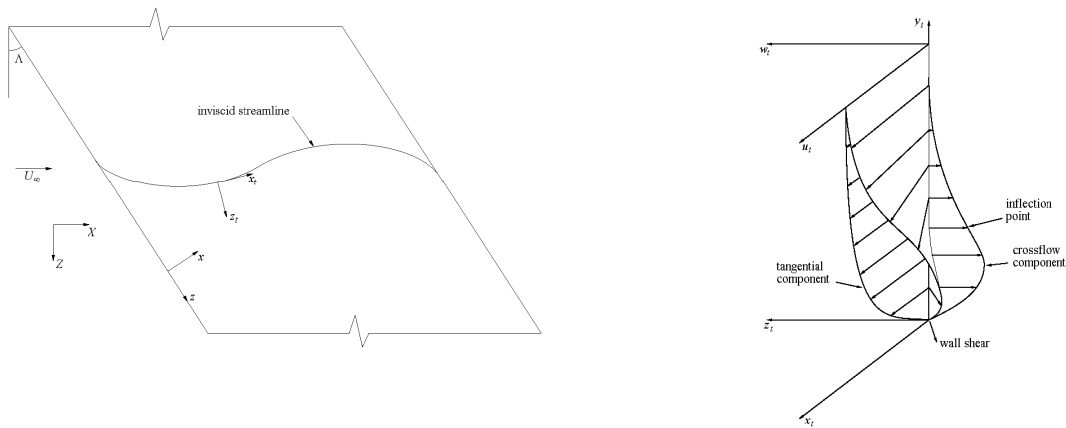


Figure 1. Flow over a swept wing and the resolved local streamwise and crossflow boundary-layer profiles. Note the inflection point in the crossflow profile.

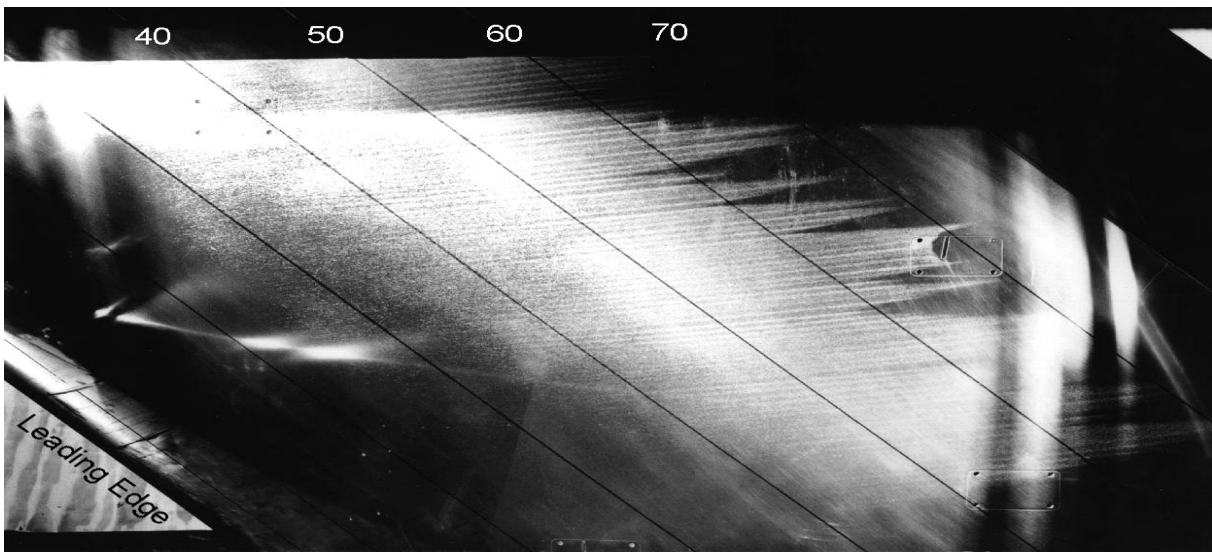


Figure 2. Flow over a swept wing in a quiet wind tunnel showing the stationary pattern of the crossflow instability characteristic of flight (Radeztsky et al., 1993).

1.1 Linear Stability Theory

Linear stability theory *alone* is not so successful for 3-D boundary layers. Arnal (2009) reviews the different approaches to the application of the e^N method. When applied to available flight and wind-tunnel experiments, there is large scatter in the values of the N factor at the onset of transition among the different methods. There are three reasons for this behavior: 1) Transition

location is more difficult to determine accurately in 3-D flow than in 2-D flow. 2) Crossflow disturbances are ultra sensitive to micron-sized roughness elements which have no effect on streamwise disturbances (Radeztsky et al., 1993). 3) Disturbance development can be dominated by nonlinearities during a large part of the transition process and the use of linear theory up to breakdown is inappropriate and can overestimate wave amplitude (Reibert et al., 1996; Haynes & Reed, 2000).

Unlike T-S instabilities, the crossflow problem exhibits stationary as well as traveling disturbances that are amplified. Even though both types of waves are present in typical swept-wing or rotating-disk flows, transition is usually caused by either the stationary or the traveling waves. Although linear theory predicts that the traveling disturbances have higher growth rates, transition in many experiments is induced by stationary waves. Whether stationary or traveling waves dominate is related to the receptivity process. Stationary waves are more important in low-turbulence environments characteristic of flight, while traveling waves dominate in high-turbulence environments (Bippes 1997; Deyhle & Bippes 1996). In the flight environment, the presence of micron-sized 3-D roughness at the leading edge (e.g. from a painted surface) establishes the stationary streamwise vortex. In fact, the 3-D boundary layer is ultra sensitive to this roughness, yet this roughness has no effect on streamwise disturbances (Radeztsky et al., 1993). In interacting with inherent surface roughness, freestream turbulence appears to be the source of travelling crossflow, but freestream turbulence is not a dominant feature of flight conditions (White & Saric 2005). Therefore, in flight, the instability appears as stationary co-rotating vortices whose axes are aligned to within a few degrees of the local inviscid streamlines. The wavelength of these vortices is approximately four times the local boundary-layer thickness. See Figure 2.

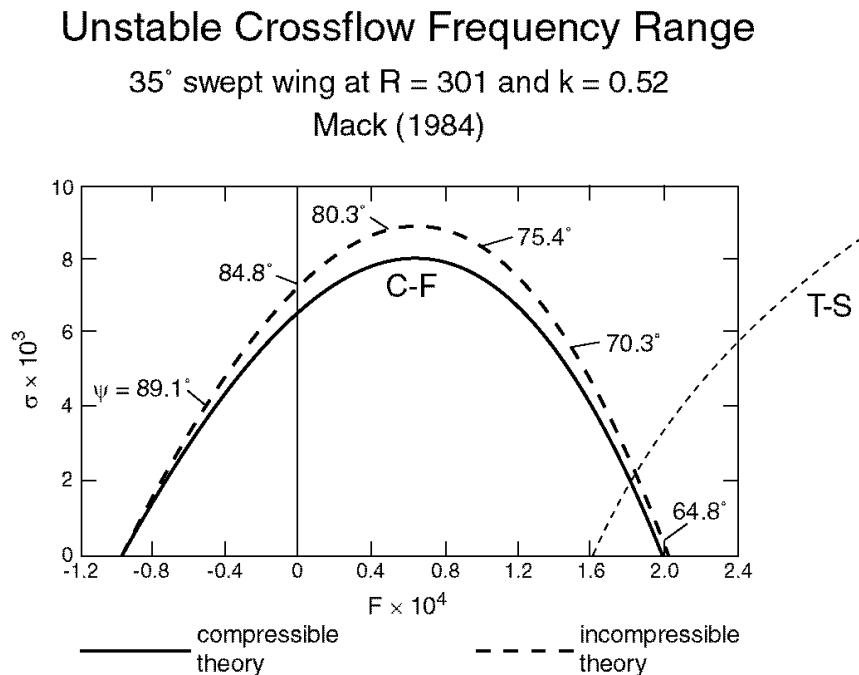


Figure 3. Typical linear stability theory results for crossflow show that traveling disturbances have higher growth rates (Mack 1984).

One of the important results to come out of the DLR group is the set of data that show early saturation of the disturbance amplitude and the failure of linear theory to predict the growth of the instability. They also report distorted mean profiles similar to those of Kohama et al. (1991) and Malik et al. (1994) due to the presence of the stationary corotating vortices. A similarity between the DLR and ASU experiments is the high N -factors and high amplitude of the mean-flow distortion (10%-20%). It is not surprising that linear theory fails.

For low-amplitude crossflow waves, Radeztsky et al. (1994) find that linear stability theory correctly predicts the expected wavelengths and mode shapes for stationary crossflow, but not the growth rates. For this case, Haynes and Reed (2000) find that LPSE including curvature correctly predicts the wavelengths, mode shapes, and growth rates. As discussed in the following Section, this is not the case for higher-amplitude crossflow and the results of Reibert et al. (1996) and Haynes & Reed (2000) demonstrate conclusively that a nonlinear calculation is required to obtain complete agreement. This is shown in the next section.

1.2 Parabolized Stability Equations

The NPSE approach has recently been validated for 3-D flows subjected to crossflow disturbances by Haynes & Reed (2000). Here a detailed comparison of NPSE results with the experimental measurements of Reibert et al. (1996) show remarkably good agreement. The configuration is an NLF(2)-0415 45°-swept airfoil at -4° angle-of-attack, so chosen to provide an extensive region of crossflow (at least back to mid-chord) for detailed study of the physics. A spanwise array of roughness elements is used near the airfoil leading edge (at 2% chord) to introduce spanwise-periodic crossflow disturbances into the boundary layer. According to LST, a spanwise spacing of 12 mm corresponds to the most highly amplified stationary crossflow disturbance. The walls of the ASU Unsteady Wind Tunnel were shaped to achieve a spanwise-independent basic-state flow – an “infinite wing” in CFD terms. The freestream turbulence are

well documented to be $O(10^{-4})$ so that, with any surface roughness, stationary crossflow is expected. Reibert et al. (1996) provide all the details for the experimental facility and set-up.

Haynes and Reed (2000) used a panel-method code to compute the inviscid flow, from which the edge boundary conditions were generated for the boundary-layer code. Agreement between the experimental and computational C_p distribution is good.

As a baseline case to study the evolution of crossflow vortices, roughness elements with a spanwise spacing of 12 mm were placed on the experimental model. The initial conditions for the NPSE calculation (with curvature) were obtained by solving the local LST equations at 5% chord location for the fundamental [mode (0,1)] and adjusting its RMS amplitude such that the total disturbance amplitude matched that of the experiment at 10% chord. The NPSE was then marched from 5% to 45% chord. Transition occurred on the experimental model at 52% chord.

The primary and higher modes all grow rapidly at first and saturate at about 30% chord. This is due to a strong nonlinear interaction among all the modes over a large chordwise distance. From about 35% chord on, there is still strong nonlinear interaction among the primary and second harmonic, but not the others. The development of crossflow occurs in two stages. The first stage is linear and is characterized by small vertical v and spanwise w disturbance velocities convecting low-momentum fluid away from the wall and high-momentum fluid toward the wall. This exchange of momentum occurs in a region very close to the wall where there are large vertical gradients in the basic-state streamwise velocity. Because of this large gradient, the small

displacements caused by the v and w disturbance components quickly lead to large disturbances u superposed on the basic state further downstream. This u component soon becomes too large and nonlinear interactions must be included in any calculations. This is the second stage, evidenced by roll-over seen in the streamwise-velocity contours. Figure 4 shows a comparison of the experimental and computational total streamwise velocity contours at 45% chord; the agreement between the NPSE and the experiments is excellent. Figure 5 shows the comparison of the experimental N -factor curves with LPSE (with curvature), NPSE (with curvature), and LST (with curvature). It is clear that the linear theories fail to accurately describe the transitional flow for this situation.

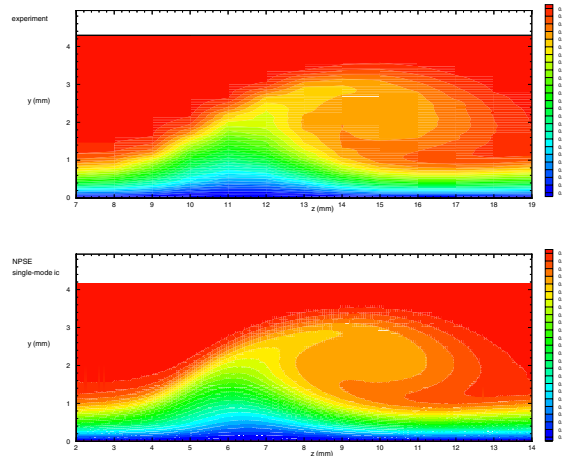


Figure 4. Streamwise-velocity contours for a swept wing showing the nonlinear distortion due to the stationary crossflow vortex pattern typical of flight. Example of successful validation: Top figure – experiments of Reibert et al. 1996; lower figure – computations of Haynes & Reed (2000).

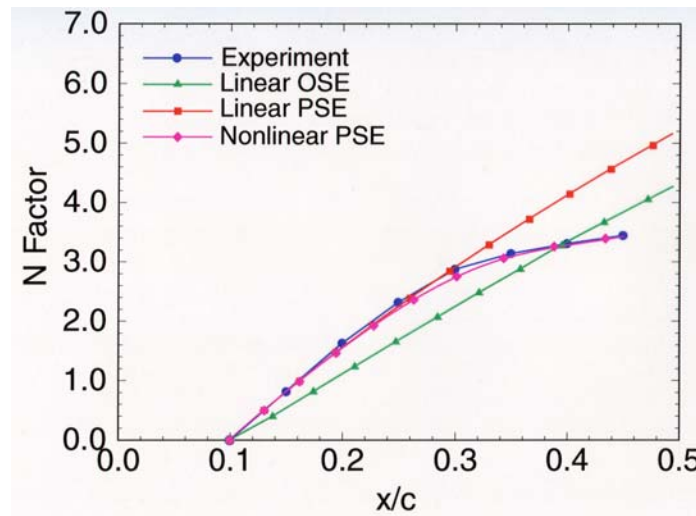


Figure 5. N-factor comparisons. NPSE agrees with experiments. LST (with curvature) underpredicts initial growth and overpredicts growth after nonlinear effects set in. LPSE (with curvature and nonparallel) successfully predicts initial growth but is quickly in error after nonlinear effects set in. Experiments: Reibert et al. 1996; computations: Haynes & Reed 2000.

There has been much debate about the effects of curvature. For this configuration, the inclusion of curvature has a very small effect on the metric coefficients. The maximum values of k_1 and k_2 occur at 5% chord where they are the order of 1.01 and 10^{-3} , respectively. They both drop off sharply with increasing chordwise distance. These values may compel the researcher to neglect curvature, but the work of Haynes and Reed (2000) demonstrates conclusively that small changes in the metric coefficients can have a significant effect on the development of crossflow vortices. Radeztsky et al. (1994) studied the effects of angle-of-attack (AOA). Here, in a case of weak favorable pressure gradient, the experiments showed that the crossflow disturbance is decaying in disagreement with various linear theories (LST, LPSE/without curvature, and LST/with curvature) that predicted the disturbance to be growing. Radeztsky et al. (1994) concluded that the disagreement was due to nonlinearity. For this case, Haynes and Reed (2000) demonstrated that the LPSE/with curvature and NPSE/with curvature both agreed with the experiment, indicating that in fact the crossflow disturbance decays and there is a strong sensitivity to changes in curvature, nonparallel effects, and pressure gradient (AOA). The disturbance was linear for this case.

Saric et al. (1998) observed that unstable waves occur only at integer multiples of the primary disturbance and no subharmonic disturbances are destabilized. They investigated the effects of distributed roughness whose primary disturbance wavenumber does not contain a harmonic at 12 mm (the most unstable wavelength according to linear theory). In the absence of artificial roughness, transition occurs at 71% chord. Adding roughness with a spanwise spacing equal to the wavelength of the linearly most unstable wave moves transition forward to 52% chord. However, subcritical forcing at 8 mm spanwise spacing actually delays transition beyond the pressure minimum and onto the trailing-edge flap at 80% chord. The NPSE results confirmed this effect.

1.3 Control with Distributed Roughness

Two important observations concerning the distributed roughness results of Reibert et al (1996) are: (1) unstable waves occur only at integer multiples of the primary disturbance wavenumber; (2) no subharmonic disturbances are destabilized. Spacing the roughness elements with wavenumber $k = 2\pi/\lambda$ apart, excites harmonic disturbances with spanwise wavenumbers of $2k$, $3k$, \dots , nk (corresponding to $\lambda/2, \lambda/3, \dots, \lambda/n$) but does not produce any unstable waves with “intermediate” wavelengths or with wavelengths greater than λ .

Following this lead, Saric et al (1998) investigate the effects of distributed roughness whose primary disturbance wavenumber does not contain a harmonic at $\lambda_s = 12$ mm (the most unstable wavelength according to linear theory). By changing the fundamental disturbance wavelength (i.e., the roughness spacing) to 18 mm, the velocity contours clearly showed the presence of the 18 mm, 9 mm, and 6 mm wavelengths. However, the linearly most unstable disturbance ($\lambda_s = 12$ mm) has been completely suppressed. Moreover (and consistent with all previous results), no subharmonic disturbances are observed. This shows that an appropriately designed roughness configuration can, in fact, inhibit the growth of the (naturally occurring) most-unstable disturbance. When the disturbance wavelength was forced at 8 mm, the growth of all disturbances of greater wavelength was suppressed. The most remarkable result obtained from the subcritical roughness spacing is the dramatic affect on transition location: In the absence of artificial

roughness, transition occurs at 71% chord. Adding roughness with a spanwise spacing equal to the wavelength of the linearly most unstable wave moves transition forward to 47% chord. However, subcritical forcing at 8 mm spanwise spacing actually delays transition beyond the pressure minimum and well beyond 80% chord (the actual location was beyond view). This promising technique has currently been demonstrated in flight on the O-2A at Texas A&M at chord Reynolds numbers of 7.5 million and on the NASA Dryden F-15B at supersonic speeds. (Saric et al. 2004; Saric et al. 2008; Rhodes et al. 2008).

Subsequent to the experiments, the NPSE results (Haynes & Reed 2000) confirmed this effect. In a DNS solution, Wassermann & Kloker (2002) have shown the same stabilization due to subcritical forcing. Using the same independent approach regarding the calculation of the basic state, they demonstrated the stabilization due to subcritical roughness and coined the name transition delay by “upstream flow deformation.”

1.4 Secondary Instabilities

Once stationary vortices reach saturation amplitude, this state can persist for a very significant streamwise distance. The velocity contours show low-momentum fluid above high-momentum fluid which produces a double inflection point in the wall-normal velocity profile. There is also an inflection point in the spanwise profile. These inflection points are high in the boundary layer and the saturated vortices become unstable to a high-frequency secondary instability that ultimately brings about transition to turbulence. Because of the importance of the secondary instabilities in determining the location of breakdown of the laminar flow, there have been a number of investigations, both experimental and computational, in this area. Bippes (1999) includes details on the German efforts, in particular, the work by Lerche (1996) that emphasizes secondary instabilities in flows with higher turbulence levels and traveling crossflow waves. Recent efforts involving secondary instabilities in the Russian traveling wave experiments are covered by Boiko et al (1995, 1999).

The first crossflow experiment for which a high-frequency disturbance was observed prior to transition was by Poll (1985). Traveling crossflow waves were observed with a dominant frequency of 1.1 kHz for $Re_c = 0.9 \times 10^6$. Increasing the chord Reynolds number to 1.2×10^6 increased the traveling crossflow frequency to 1.5 kHz and also included an intermittent signal at 17.5 kHz superposed on the underlying traveling crossflow waves. Poll noted that increasing the Reynolds number beyond 1.2×10^6 resulted in turbulent flow at the measurement location, so the high-frequency signal appeared only in a narrow range just prior to transition. Poll attributed the existence of the high-frequency component to intermittent turbulence.

A high-frequency secondary instability was specifically investigated as a source of breakdown by Kohama et al (1991). This experiment combined hotwire measurements and flow visualizations and was intended to determine the location and behavior of the secondary instability mode relative to visualized breakdown patterns. It is clear from the Kohama et al (1991) experiments that there is a growing high-frequency mode in the region upstream of transition that can be associated with an inviscid instability of the distorted mean flow. However, a concern can be raised because the measurements were made without a well-controlled primary disturbance state. Experiments subsequent to this work used arrays of micron-sized roughness elements near the leading edge that established the spanwise uniformity both of the stationary vortex amplitudes and the transition location. Without the benefit of this technique, the data obtained by Kohama et al (1991) likely spanned a wide range of stability behavior despite having been obtained at a single chord position. Improvements in experimental techniques mean that more recent secondary

instability experiments have replaced the work by Kohama et al (1991) as the best source for secondary instability data.

Kohama et al (1996) provide somewhat more detail than Kohama et al (1991) by including velocity fluctuation maps that are filtered to give either primary instability or secondary instability fluctuation levels. Kohama et al (1996) conclude that a “turbulent wedge starts from the middle height of the boundary layer” and that this behavior is different from the usual picture of a turbulent wedge that originates in the high-shear regions in naphthalene flow-visualization experiments. A subsequent swept plate experiment by Kawakami et al (1999) was conducted to further refine these measurements. Kawakami et al’s experiment featured a small speaker mounted flush with the surface that permitted tracking of particular secondary-instability frequencies. Without acoustic forcing, two separate high-frequency bands of disturbances were observed to be unstable. At a chord Reynolds number of 4.9×10^6 , a band located between 600 Hz and 2.5 kHz destabilized just downstream of $x/c = 0.35$ and a second band located between 2.5 and 4.0 kHz destabilized just upstream of $x/c = 0.50$. Transition was observed around $x/c = 0.70$. With acoustic forcing applied, the secondary instability frequency with the largest growth between $x/c = 0.40$ and $x/c = 0.475$ was observed to be 1.5 kHz.

In an effort to provide a more concrete experimental database on the behavior of the secondary instability, White & Saric (2005) conduct a very detailed experiment that tracks the development of secondary instabilities on a swept wing throughout their development for various Reynolds numbers and roughness configurations. They found a number of unique secondary instability modes that can occur at different frequency bands and at different locations within the stationary vortex structure. In White & Saric’s experiment as many as six distinct modes are observed between 2 and 20 kHz. The lowest-frequency mode is nearly always the highest amplitude of all the secondary instabilities and is always associated with an extremum in the spanwise gradient, $\partial U/\partial z$ which Malik et al (1996, 1999) refer to as a mode-I or z mode. Higher frequency modes include both harmonics of the lowest-frequency z mode that appear at the same location within the vortex and also distinct mode-II or y modes that form in the $\partial U/\partial y$ shear layer in the portion of the vortex farthest from the wall. The lowest frequency mode is typically detected upstream of any of the higher frequency modes. However, many higher frequency modes appear within a very short distance downstream. All of the secondary instability modes are amplified at a much greater rate than the primary stationary vortices (even prior to their saturation). The rapid growth leads very quickly to the breakdown of laminar flow, within about 5% chord of where the secondary instability is first detected. A consequence of this for transition-prediction methodologies is that adequate engineering predictions of transition location could be obtained from simply identifying where the secondary instabilities are destabilized because they lead to turbulence in such a short distance downstream of their destabilization location. An interesting feature of the breakdown of the stationary vortex structure is that it is highly localized. Spectra obtained by White & Saric at various points within the structure indicate that the first point to feature a broad, flat velocity-fluctuation spectrum characteristic of turbulence is a point very close to the wall in the region of highest wall shear. Other points in the structure remain essentially laminar for some distance downstream of the initial breakdown location. This finding supports the notion of a turbulent wedge originating near the wall, not what was concluded by Kohama et al (1996).

A successful computational approach to the secondary instability was presented by Malik et al (1994) who used a NPSE code to calculate the primary instability behavior of stationary disturbances of a swept Hiemenz flow. As described previously, the NPSE approach successfully captures the nonlinear effects including amplitude saturation. The distorted meanflow provides a basic state for a local, temporal secondary instability calculation. The most unstable frequency is approximately one order of magnitude greater than the most unstable primary traveling wave

similar to Kohama et al (1991) and the peak mode amplitude is “on top” of the stationary crossflow vortex structure. This location corresponds to what will be referred to below by Malik et al (1996) as the mode-II secondary instability.

In order to obtain a more direct comparison to experimental data, Malik et al (1996) used parameters designed to match the conditions found for the swept-cylinder experiment of Poll (1985) and the swept-wing experiment of Kohama et al (1991). The calculations of Malik et al (1996) reveal that the energy production for a mode-I instability is dominated by the term $\langle u_2 w_2 \rangle \partial U_2 / \partial z_2$ and the mode-II instability is dominated by $\langle u_2 v_2 \rangle \partial U_2 / \partial y_2$ where the subscript “2” refers to a primary-vortex-oriented coordinate system. This energy-production behavior suggests that the mode-I instability is generated primarily by inflection points in the spanwise direction and the mode-II instability is generated by inflection points in the wall-normal direction. This situation is analogous to the secondary instabilities of Görtler vortices (Saric 1994). Malik et al (1996) claim that the fluctuations observed by Kohama et al (1991) are mode-II instabilities but the spectral data presented by Kohama et al (1991) likely includes contributions of both the type-I and type-II modes. Although one or the other production mechanism may dominate for a particular mode, it is too simplistic to assume that only the spanwise or wall-normal inflection points are responsible for the appearance of a particular mode; with such a highly distorted 3-D boundary layer, all possible instabilities must be evaluated.

Malik et al (1996) also compute the secondary instability behavior observed by Poll (1985) and predict a 17.2-kHz mode compared to Poll's high-frequency signal occurred at 17.5 kHz. Based on the shape of this disturbance, Malik et al claim that this is a type-II mode. The same approach is applied by Malik et al (1999) to the swept wing experiments of Reibert et al (1996). Malik et al (1999) again apply a local, temporal stability of the stationary crossflow vortices that are established by the primary instability and find that better transition correlation results can be obtained by following the growth of the secondary instability in an N-factor calculation than simply basing a prediction on the location at which the secondary instability destabilizes. A method based on the primary instability alone cannot adequately predict transition location.

An alternative to the approach used by Malik et al (1994, 1996, 1999) is presented by Koch et al (2000) who find the nonlinear equilibrium solution of the primary flow. Koch et al use the nonlinear equilibrium solution as a receptivity-independent basic state for a Floquet analysis of secondary instabilities of the saturated vortices. Yet another approach is by Janke & Balakumar (2000) who use a NPSE for the base flow and a Floquet analysis for the secondary instabilities. Both Koch et al (2000) and Janke & Balakumar (2000) are in general agreement with the various computations of Malik and coworkers.

A DNS approach to the problem of the stationary-vortex saturation and the ensuing secondary instability was pursued by Högberg & Henningson (1998). These authors impose an artificial random disturbance at a point where the stationary vortices are saturated. These disturbances enhance both the low- and high-frequency disturbances downstream, and each frequency band has a distinct spatial location, with the high-frequency disturbance located in the upper part of the boundary layer and the low-frequency disturbance located in the lower part. Spectral analysis of the resulting disturbance field shows that the most-amplified high frequency is somewhat more than an order of magnitude higher frequency than the most-amplified traveling primary disturbance. Another high-frequency peak at approximately twice this frequency is also evident in the spectra. This peak likely corresponds to a type-II mode, although this feature is not described by the authors.

Another very highly resolved DNS study of nonlinear interactions of primary crossflow modes, their secondary instabilities, and eventual breakdown to turbulence is by Wassermann & Kloker (2002). Wassermann & Kloker emphasize disturbance wave packets that may be more realistic than single-mode disturbances. One of the most important findings obtained from the wave-packet approach is that unevenly spaced primary vortices of differing strengths can interact in such a way to bring about an earlier onset of secondary instabilities and breakdown than would be found from a single-mode disturbance. Also, Wassermann & Kloker find that when the forcing that initiates the high-frequency secondary instability in their simulation is removed, the secondary-instability disturbances are convected downstream, out of the computational domain. This indicates that the secondary instability is convective and that the explosiveness of the secondary instability's growth is not associated with an absolute instability. The advantage of Wasserman & Kloker's DNS solution is its ability to reveal the rather intimate details of the breakdown process. As such, the work is one of the foundation contributions.

At this time, the various approaches to the secondary instability problem, experimental, nonlinear PSE, and DNS, have achieved rather remarkable agreement in terms of identifying the basic mechanisms of the secondary instability, unstable frequencies, mode shapes, and growth rates. A comparison of three of the most recent efforts is shown in Figure 6. This comparison shows agreement on the location of the breakdown and that it is associated with an inflection point in the spanwise direction (an extremum in $\partial U/\partial z$).

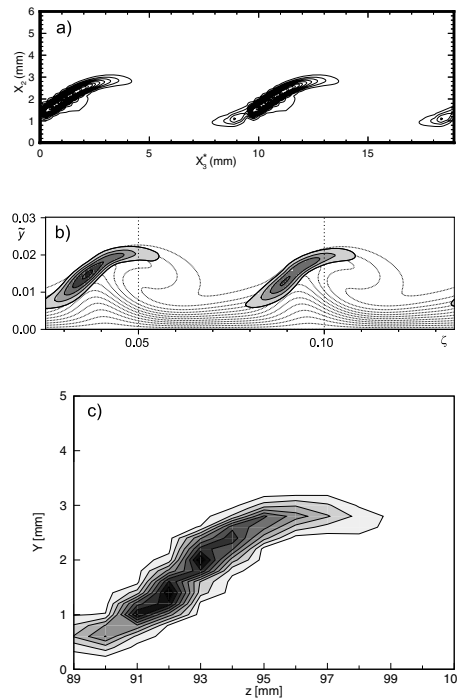


Figure 6. Mode-I velocity fluctuation contours. (a) NPSE (Figure 7 from Malik et al 1999), (b) DNS (Figure 20b from Wassermann & Kloker 2002), and (c) Experiment (Figure 11 from White & Saric 2005).

1.5 Summary

The DNS and NPSE with curvature for 3-D crossflow-dominated flows have shown very encouraging results in validating against the available carefully documented experimental databases, but more work is still needed to simulate physical initial conditions including the freestream and leading-edge surface roughness. The flight experiments of Carpenter et al (2009) are beginning to provide receptivity data for roughness in flight to provide these much needed upstream conditions for the calculations.

2.0 Attachment Line

The attachment-line boundary layer (see Figure 7) can undergo an instability, or be subject to contamination by wing-root turbulence; these phenomena are associated with, in general, swept wings with a large leading-edge radius (Pfenninger 1965, Cumpsty and Head 1967, Gaster 1967, Pfenninger and Bacon 1969, Poll 1979, Hall et al. 1984, Reed & Saric 1989).

Control in this case is achieved by limiting the value of the attachment-line momentum-thickness Reynolds number. The initial flow condition at the root of the wing determines the critical attachment-line momentum-thickness Reynolds. Many experiments have been done to find critical Reynolds number values for both attachment-line stability and leading-edge contamination.

If the wing root is contaminated with turbulence from the fuselage or some other structure (pylons, for instance), the disturbances feeding into the boundary layer are relatively large and there exists an attachment-line momentum-thickness Reynolds below which the turbulent flow disturbances are damped and the flow becomes laminar. To avoid leading-edge contamination, that is, disturbances propagating along the attachment line and feeding into and tripping the boundary layer, it is necessary to keep the attachment-line Reynolds number $Re_{\theta AL}$ below 100 (Pfenninger 1965).

$$Re_{\theta AL} = 0.404 [Re' r \tan \Lambda \sin \Lambda / (1 + e)]^{1/2} \leq 100$$

where Re' is the dimensional unit Reynolds number based on freestream conditions, r is the dimensional normal-to-the-LE radius, Λ is the leading-edge sweep angle, and e is the ellipticity of the LE ($e = 0$ is conservative). Thus a finite radius is possible.

On the other hand, if the flow is laminar at the root or if turbulent disturbances have been removed by suction near the wing root or by some device such as a Gaster bump, then above a certain value of Re_0 small disturbances seem to grow and result in a turbulent attachment line. This is called attachment-line stability, and the current suggested design criterion is

$$Re_{\theta AL} = 0.404 [Re' r \tan \Lambda \sin \Lambda / (1 + e)]^{1/2} \leq 245$$

For attachment-line stability, Gaster (1967) performed experiments on a Handley Page laminar flow wing at 43° sweep which indicated that the critical Reynolds number for a laminar boundary layer (small disturbances) was greater than 170 (the highest Re_0 used in the experiment). Gaster also designed a bump which bears his name, the purpose of which is to remove the turbulent boundary layer originating at the wing root to help stabilize the flow. Cumpsty and Head (1969) conducted experiments on a swept wing model showing that laminar flow is stable up to $Re_{\theta AL}=245$. Pfenninger and Bacon (1969) performed experiments on a 45° swept airfoil and

found the critical $Re_{\theta AL}$ for laminar flow is 240. The experiments by Poll (1979) indicated that laminar flow was stable to $Re_{\theta AL} = 230$. A good general value for the onset of transition for an uncontaminated root flow is $Re_{\theta AL} = 240$.

Under ordinary circumstances, in practice for transport flight, one is dealing with leading-edge contamination and one selects the sweep angle and *normal-to-the-LE radius* so that the attachment-line Reynolds number is well below 100. Otherwise, one has tripped the boundary-layer from the leading edge. Here is an opportunity to use a Gaster bump or simple passive suction patch near the wing root. Now one is dealing with attachment-line stability, with the attachment-line Reynolds number criterion now being relaxed to needing to be maintained below 245. In this case one has the flexibility to increase the nose radius by a factor of 6.

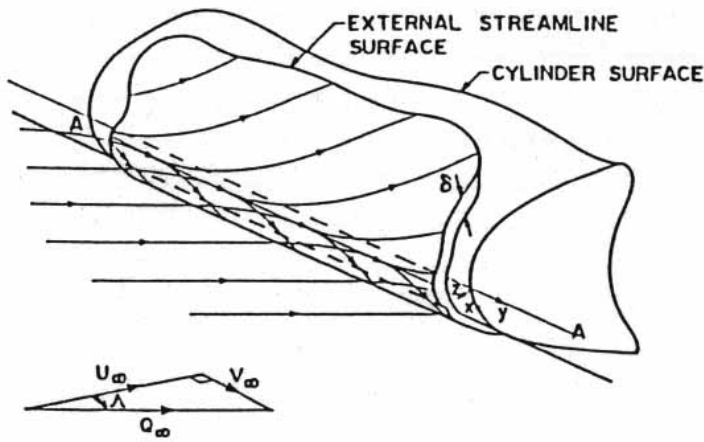


Figure 7. Flow around swept wing attachment line

Several investigators have used DNS and linear and nonlinear analysis techniques to look at the nature of the instabilities and to confirm previous experimental results. Hall, Malik, and Poll (1984) used nonparallel linear stability theory on a swept Hiemenz (stagnation point) flow and predicted a critical $Re_{\theta AL} = 245$. Spalart (1989) used a DNS method to confirm this result. Hall and Malik (1986) attempted to bridge the gap between the turbulent and laminar originating flow by using weakly nonlinear theory and DNS, and found that subcritical disturbance growth corresponds to branch II of the neutral curve. Eigenvalue analysis of Lin and Malik (1996, 1997), and DNS work by Joslin (1995, 1996) has confirmed previous results.

Although empirical, the use of the attachment-line momentum-thickness Reynolds number has been demonstrated to be valid in a wide range of flows from low-speed to supersonic. Analytical, computational, and experimental attempts to characterize attachment line transition have historically reduced to this criterion. At this point this seems to be the best available engineering strategy for predicting transition on the attachment line.

SUPERSONIC FLOWS

Considerable uncertainty exists in both the prediction and control of transition in supersonic flows due to the dearth of reliable experiments. The paper by Mack (1984) is the most complete description of compressible stability available anywhere. The linear stability analysis of high-speed boundary layers uncovers three major differences between it and the subsonic analysis: the presence of a generalized inflection-point, the dominance of 3-D viscous disturbances, and

multiple acoustic modes (Mack Modes). Stability analyses of high-speed boundary layers have largely been limited to simple geometries such as flat plates and axisymmetric cones.

3.0 STABILITY ANALYSES

3.1 Generalized Inflection-Point Criterion

The boundary layer on an adiabatic flat plate in a compressible flow always features $D(\rho DU) = 0$ somewhere in the flow. Thus, even zero-pressure-gradient flows are subject to inviscid instabilities that grow with increasing Mach number. As y_s moves away from the wall with increasing Mach number, the range of unstable frequencies is enlarged at high Reynolds numbers. This effect occurs up to a Mach number of approximately 5. In contrast to $M=0$, when viscosity is considered at $M>1$, it may be stabilizing relative to the dynamic instability.

3.2 3-D Viscous Disturbances

In the supersonic case ($1 < M_e < 10$) under perfect gas assumptions, Mack completed extensive linear stability computations of 3-D stability maps on a flat plate and found many important results (see Mack 1984 for the details and comparisons with experiment). The earliest results showed that above a Mach number of 1, 3-D waves corresponding to the first viscous mode have a larger amplification factor than the corresponding 2-D disturbance. In 1970's, Mack validated Kendall's experiments (in the JPL 20" Variable Mach Number Supersonic Tunnel) showing dominance of 3-D viscous modes up to Mach 4 on a flat plate. The dominance of 3-D viscous disturbances refers to the fact that at supersonic speeds, the 2-D viscous disturbances called Tollmien-Schlichting (TS) waves at lower speeds are not the most unstable viscous disturbances. Instead, oblique disturbances of the same general family are most amplified. These are called first-mode disturbances. As the Mach number is increased above 1, the most unstable wave angle quickly increases to 45° at $M_e = 1.3$, 55° at $M_e = 1.6$, and 60° at $M_e = 2.2$. Thus, the assumption of 2-D viscous disturbances cannot be made in supersonic flows.

3.3 Multiple Acoustic Modes: Mack Modes

One of the most significant developments in compressible theory comes from Mack, who discovered a new family of solutions to the compressible equations. They can be explained by considering the inviscid stability equation in the form

$$\partial^2 \psi / \partial y^2 + (1 - M^2) \partial^2 \psi / \partial x^2 + f(M, \psi, \partial \psi / \partial y) = 0$$

where

$$\psi = v / (\alpha U + \beta W - \omega)$$

$$M = (\alpha U + \beta W - \omega) M_e / [(\alpha^2 + \beta^2) T]^{1/2}$$

$M(y)$ is the relative Mach number between the local basic-state velocity and the propagation speed of a neutral wave. M_e is the edge Mach number. Here, we recall that and take advantage of the fact that $\partial^2 \psi / \partial x^2$ was the source of $-(\alpha^2 + \beta^2) \psi$ in the disturbance equation. Obviously, when $M^2 < 1$, this equation is elliptic and the eigenvalue is unique as it is in the case of incompressible inviscid theory. When $M^2 > 1$, this equation is hyperbolic and an infinite discrete set of eigenvalues can satisfy the boundary conditions. $M^2 = 1$ at $y = y_a$ in the boundary layer

and y_a is called a turning point. The solution of this equation can be found by using WKB methods. For $y < y_a$, the solutions are oscillatory and for $y > y_a$ they are exponential.

Physically, the disturbances propagate at a speed that is subsonic relative to the edge velocity, but supersonic relative to the region near the wall ($y < y_a$). Thus, for an adiabatic flat plate with $M_e = 3.8$, disturbances with phase speeds $c_r > 0.5$ are supersonic with respect to the wall region (Morkovin 1991). At the same phase speed c_r , a sequence of wavenumbers satisfy the differential equation and boundary conditions. These extra solutions are higher modes and are most unstable as 2-D waves, because it is then that the relative supersonic region is of maximum extent. They have shorter wavelengths than the usual T-S instability waves (first modes) since the wavenumber sequence is approximately

$$2\alpha_n/\pi = 1, 3, 5, 7, \dots$$

They are not T-S waves by character or behavior and it is fitting that they be called Mack modes. They represent inviscid acoustic waves that reflect inviscidly between the solid wall and the relative sonic line in the boundary layer. See also Mack (1987).

The lowest-frequency Mack mode, the so-called second mode, is found to be the dominant instability for Mach number greater than about 4; it is more unstable than either the 3-D first mode or any of the other higher modes. If $M^2 < 1$ everywhere within the boundary layer, then the first mode may be present. If $M^2 > 1$ somewhere within the boundary layer, the flow is unstable to “Mack” modes. The second mode is a “subsonic” mode in that its structure exponentially decays with height in the inviscid region of the shock layer. The second mode is found in the experiments of Kendall (1975), Demetriades (1977), and Stetson et al. (1984). Beyond these experiments, there has not been a systematic effort to validate Mack’s predictions or to investigate the conditions (roughness, bluntness, angle of attack, wall cooling, chemistry effects etc.) at which the first mode, second mode, transient growth or crossflow dominate transition.

Mack (1984) provides additional insight to second-mode behavior, discussing the effect of the thermal boundary layer. Mack observes that whereas the first mode is stabilized by cooling in air, the second mode is actually destabilized. The second mode is also found to be less stable with decreasing viscosity in air. This idea is related to the argument about cooling in that the viscosity of air increases with temperature. As temperature decreases, the local speed of sound decreases, which means the local Mach number M^2 increases and the second mode is more unstable.

Additionally Mack (1984) reasons that the behavior of the second mode is influenced by the height of the boundary layer, which is affected by both wall cooling and viscosity. There is a strong tuning with the boundary-layer thickness, so that the frequency of the most amplified disturbance may be predicted from this flow parameter. In particular, the fluctuation wavelength is approximately twice the boundary-layer thickness. This implies that if the boundary-layer thickness is changed, for example by cooling, a corresponding and predictable change in frequency should be observed. A thinning of the boundary layer decreases the wavelength and thus increases the frequency, with the converse being true.

It is apparent from the discussion of Mack (1987) that the size of the region of relative supersonic flow is an important factor in determining second-mode behavior. That is, the thickness of the region between the wall and the relative sonic line in which $M^2 > 1$ and in which the second mode is unstable, determines the characteristics of the instability. The thermal boundary-layer profile

affects both the viscosity and the local sonic speed (and thus M^2). Accordingly, particular attention should be given to the thermal boundary layer as a part of a second-mode investigation.

3.4 Comparisons

As Schneider (2001) points out, accurate depiction of the growth of a second-mode instability wave over a circular cone at zero-angle of attack remains a challenge, both computationally and experimentally. The series of experiments performed by Stetson et al. (1984), who consider the growth of instabilities on right-circular cones (both sharp and blunted) at zero-angle-of-attack at Mach 8, has provided the basis for many computational efforts. Numerical comparisons to the observed growth of second-mode instabilities over the spherically blunted-cone are reported by Malik et al. (1990), Esfahanian (1991), Kufner et al. (1993), and Rosenbloom et al. (1999). Agreement with the experimentally observed growth rates can be described as qualitative.

The Stetson et al. (1984) geometry is a 7° half-angle right-circular cone, with a blunted nose of radius 3.81 mm. The total length of the model is just over 1 m ($s = 267$). The free-stream flow is Mach 8, with zero-incidence with respect to the cone's axis. The Reynolds number (based upon free-stream conditions and the nose radius) is 3.3×10^5 . The focus of the experiment is the second-mode instability, which is thought to be dominant for high-speed flows over smooth, convex, axisymmetric geometries in two-dimensional flow.

Schneider (2001) summarizes the Stetson experimental conditions very efficiently. Paraphrasing Schneider, the total pressure is 4.00 MPa; the total temperature is 750 K. On the cone, surface measurements are taken for pressure and temperature. Basic-state profiles are measured using total-temperature and pitot-pressure probes. Basic-state comparisons between experimentally determined profiles and computed profiles are discussed below. For the Stetson experiment, disturbances are measured using a series of four hot-wire anemometers. Starting at 0.254 m ($s = 66.7$), disturbance spectra are measured through 0.922 m ($s = 242$). The measured total-temperature spectra are shown in Figure 11; here $\omega = 1$ corresponds to $f^* = 49.5$ kHz. The second-mode disturbances correspond to the spectral peaks that appear in the range $2.5 < \omega < 3$.

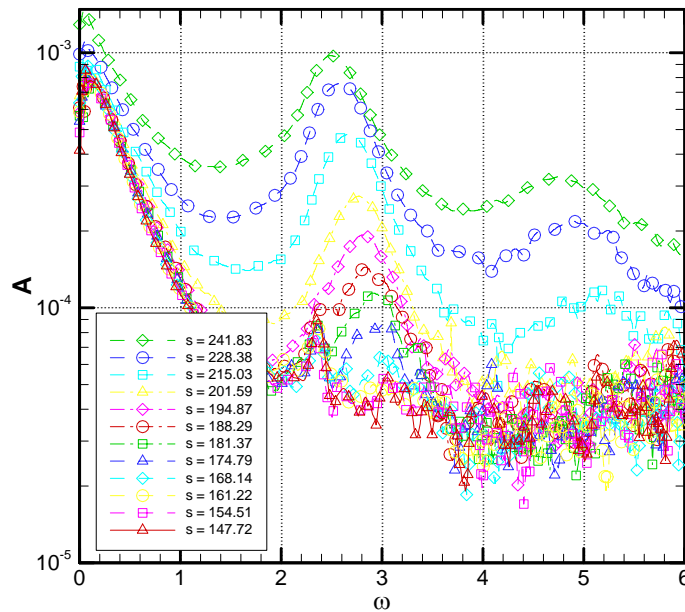


Figure 11: Stetson experiment: measured disturbance spectra of total temperature. From Lyttle et al. (2004)

From Figure 11, there follow some observations about the experiment. First, Schneider (2001) notes that the experimental (free-stream) environment is not quiet, thus Figure 11 shows the growth of broadband, uncontrolled disturbances that result from the free-stream noise. Second, one notices the presence of a harmonic of the second-mode disturbance, starting at $s = 215$. This implies that non-linear interactions may be important downstream of $s = 215$. Summing up, the validity of comparing these experimental results with linear stability theory is limited by the free-stream disturbance environment and the possible presence of non-linear interactions.

Following Malik et al. (1990), many numerical investigators have chosen $s = 175$ as the place to make a comparison with the second-mode growth-rates reported by Stetson. As seen in Figure 12, the numerically determined growth rates (including Lyttle et al. 2004) consistently peak roughly 60% higher than the peak growth-rate reported by Stetson. There have been a variety of theories to try to explain this discrepancy. Schneider (2001) points out that Stetson postulates that non-linearities are present at station 175, visible in Figure 7b in Stetson et al. (1984). It has been pointed-out that the wall temperature at $s = 175$ is not adiabatic, whereas the numerical (basic-state) models assume an adiabatic wall. Mack (1987) points out that the origin of the disturbances (receptivity) is not addressed by linear-stability theory - nor by the experiment. Furthermore, Mack (1987) points out that the experimentally determined growth rates are found using the y -locations that have the peak wide-band response - not with regard to the location of the peak of an individual frequency component. New experimental initiatives, led by Schneider et al. (2002) and Maslov (2001), address these issues.

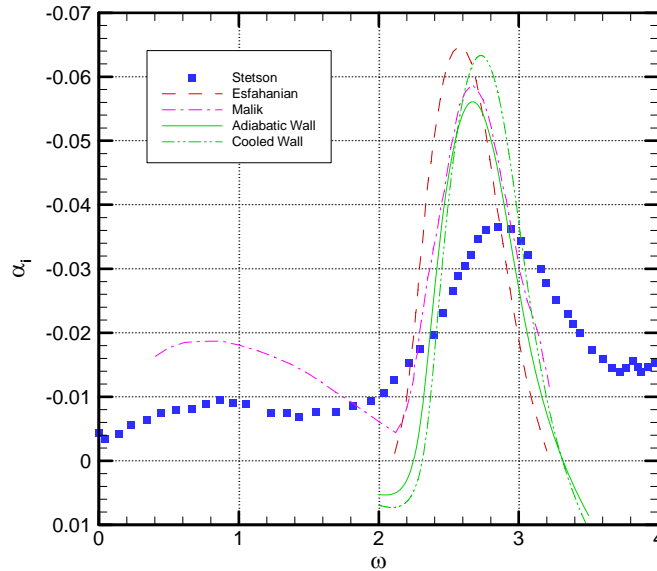


Figure 12: Second-mode growth rates as functions of frequency at $s=175$. From Lyttle et al. (2004)

Using a finite-volume code developed in-house, Lyttle et al. (2004) solve the Navier-Stokes equations for these conditions and use the solutions to perform linear-stability analyses to determine the growth of second-mode disturbances. The traditional approach for numerically investigating the Stetson et al. (1984) case is to model the cone-wall as being adiabatic. This is the standard boundary-condition used by numerical investigators, and was the intent of the Stetson experiment. As Schneider (2001) points out, this assumption is not supported by the experimental evidence. The computed adiabatic wall temperature distribution is higher than the experimentally measured temperature distributions. Schneider further observes that, as consecutive experimental runs are made, the measured temperature distribution rises from run to run, until an equilibrium temperature distribution is reached. Schneider hypothesizes that the heat capacity of the model prevents the wall temperature from reaching the adiabatic value. Lyttle et al. (2004) incorporate an option to use an experimentally determined wall-temperature distribution for the basic state.

Following the suggestion of Schneider (2001), comparisons are made of integrated growth-rates among the computations and the experiments. This may be a more appropriate comparison because the experiments measure the disturbance amplitudes, then calculate the growth-rates based on the change in disturbance amplitudes. The integrated growth-rates, N-factors, depend on the two integration-endpoints s_0 and s_1 , and are calculated as follows.

$$N = \ln\left(\frac{A_1}{A_0}\right) = \int_{s_0}^{s_1} -\alpha_i ds$$

To place the current results in the context of the Stetson experiment, the adiabatic-wall, cooled-wall, and Stetson N-factors are compared, using $s = 195$ as the reference location. The current results' agreement with the experimental results is best in the range of frequencies $2.4 < \omega < 2.8$. Examining the experimentally determined amplitudes from Figure 11, this frequency range corresponds with those frequencies that are most-amplified in the experiment.

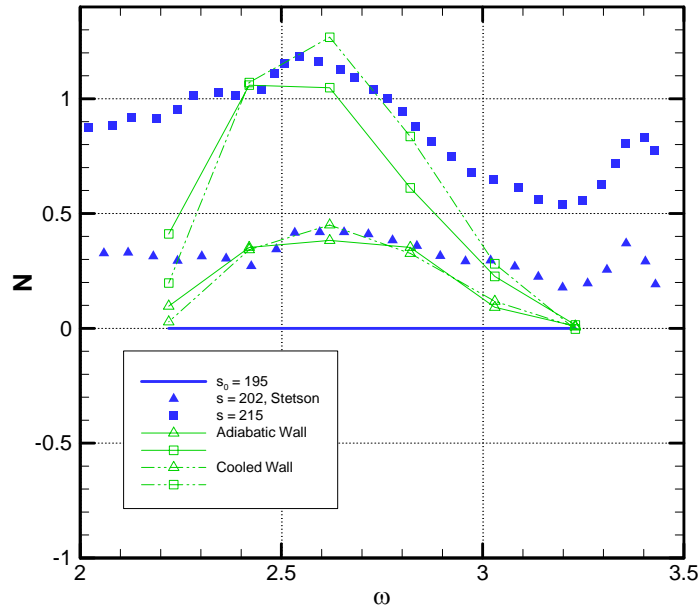


Figure 13: Comparison of N-factors, $s_0=195$, Stetson case (Lyttle et al. 2004).

The N-factor curves for a series of individual disturbance waves are considered, using $s = 195$ as the reference location. It is surmised that if a discernible linear-growth region exists, the extent of such a region can be identified by choosing $s_0 = 195$. For example, the results for $\omega = 2.62$ are shown in Figure 14, demonstrating the existence of a linear-growth region. The traditional under-prediction of growth-rates at $s = 175$ might also be explained by examining Figure 14.

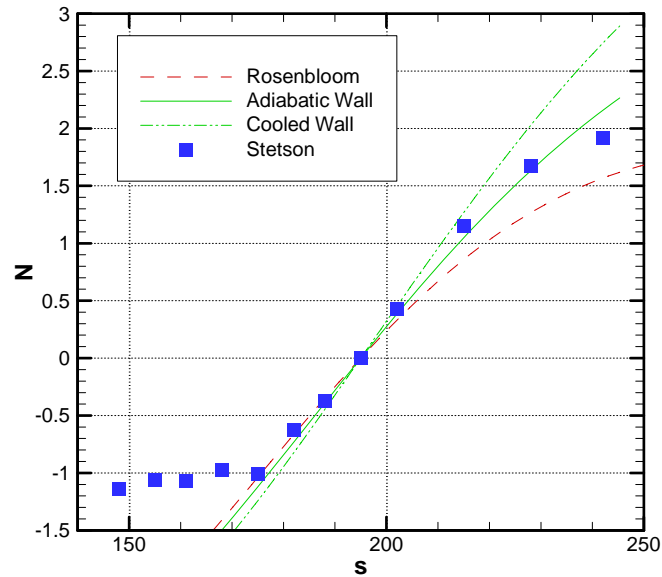


Figure 14: N-factor comparison, $\omega=2.62$, Stetson case (Lyttle et al. 2004).

Form these results, Lyttle et al. (2004) propose that linear-stability theory describes the growth of second-mode disturbances for $2.4 < \omega < 2.8$, and for the region $195 < s < 215$. The frequencies in this range correspond to the most-amplified second-mode frequencies. Upstream of $s = 195$, it is postulated that the amplified second-mode waves have not yet fully distinguished themselves from the noise. Indeed, the experimental N-factor curves suggest that the experimental-numerical disjoint at $s = 175$ may be attributed to signal-noise problems, rather than to non-linearity. For locations downstream of $s = 215$, perhaps non-linear interactions are important – behavior that cannot be captured using LST. Also, the agreement between the experiment and the current predictions appears better for the computations that use an experimentally determined wall-temperature distribution.

Next, Lyttle et al. (2004) consider the experiments conducted in the ITAM hypersonic wind tunnel T-326 by Shipliyuk, Maslov and colleagues, at a freestream Mach number of 5.95 on a 7° half-angle blunt-nosed cone. For the experiments, artificial waves are generated by a high-frequency glow discharge. For both the simulation and the experiment, 275 kHz disturbances are highly amplified. Again they find good agreement between LST and experiments in the phase speed and disturbance profiles (Figure 15), as well as for disturbance growth for the second mode (Figure 16).

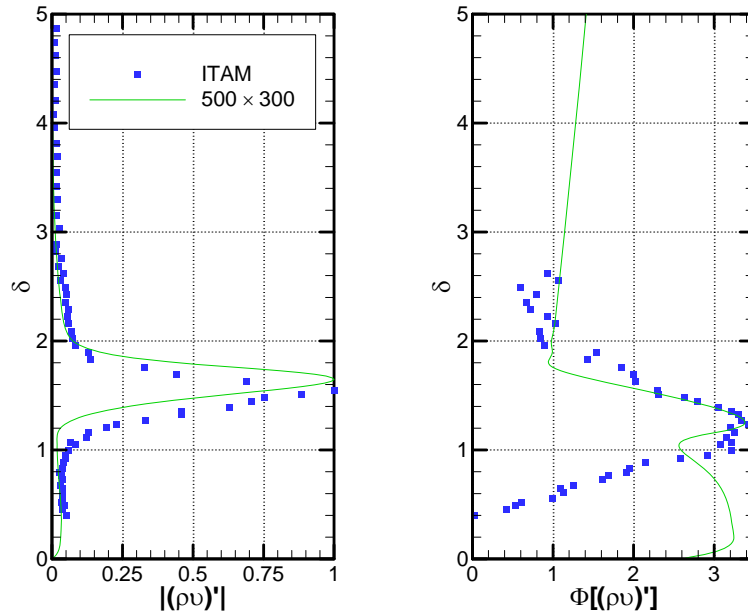


Figure 15. Comparison between ITAM experiments and LST for disturbance mass flow profile and phase within the boundary layer for the second mode. From Lyttle et al. (2004)

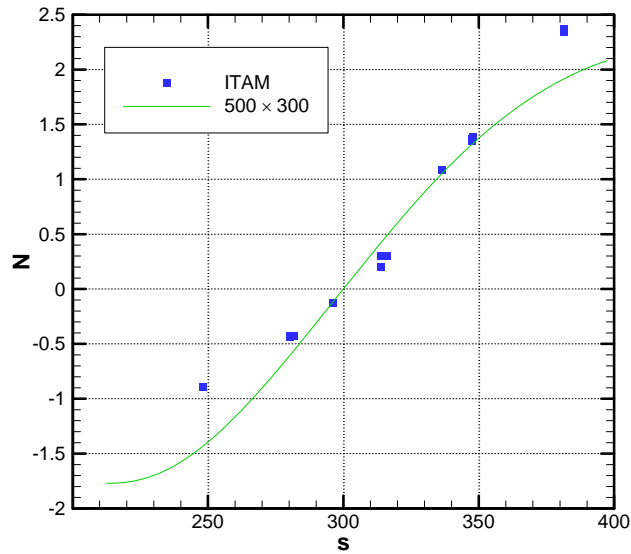


Figure 16. Comparison between ITAM experiments and LST for N-factors for the second mode. From Lyttle et al. (2004)

3.5 Summary

With little experimental validation data available for supersonic flows, validation of the physics predicted for stability and transition is difficult. It is clear that further theoretical, computational

and experimental work will have to be a joint effort in order to further identify and *validate* the appropriate models and the fundamental causes of transition. Careful, well documented validation experiments in quiet facilities and at flight conditions are very much needed – conventional facilities may even suggest trends opposite to those in flight and available flight data are uncertain in operating conditions.

REFERENCES

- [1] Arnal, D. 1997. Laminar-turbulent transition: research and applications in France, AIAA Paper 97-1905.
- [2] Arnal, D. 2009. VKI Lecture Series: Advances in Laminar-Turbulent Modeling, 12-15 January 2009, Wright State University.
- [3] Bippes, H. 1997. Environmental conditions and transition prediction in 3-D boundary layers. AIAA 97-1906.
- [4] Bippes, H. 1999. Basic experiments on transition in three-dimensional boundary layers dominated by crossflow instability. Prog. Aero. Sci. 35(4):363-412
- [5] Boiko, A.V., Kozlov, V.V., Syzrantsev, V.V., Shcherbakov, V.A. 1995. Experimental investigation of high-frequency secondary disturbances in a swept-wing boundary layer. J. App. Mech. And Tech. Phys. 36(3):385-93
- [6] Boiko, A.V., Kozlov, V.V., Syzrantsev, V.V., Shcherbakov, V.A. 1999. Active control over secondary instability in a three-dimensional boundary layer. Thermophysics and Aeromechanics 6(2):167-78
- [7] Carpenter, A.L., Saric, W.S., Reed, H.L. 2009. In-flight receptivity experiments on a 30-degree swept-wing using micron-sized discrete roughness elements. AIAA-2009-0590.
- [8] Cumpsty, N.A., Head, M.R. 1967. The calculation of three-dimensional turbulent boundary layers – Part II: attachment line flow on an infinite swept wing, The Aeronautical Quarterly, Vol. XVIII, pp. 150-164.
- [9] Cumpsty, N.A., Head, M.R. 1969. The calculation of three-dimensional turbulent boundary layers – Part III: Comparison of attachment line calculations with experiment. The Aeronautical Quarterly, Vol. XX, pp 99-113.
- [10] Demetriades, A. 1974. Hypersonic viscous flow over a slender cone, part III: laminar instability and transition. AIAA Paper No. 74-535.
- [11] Deyhle, H., Bippes, H. 1996. Disturbance growth in an unstable 3-D boundary later and its dependence on environmental conditions. JFM 316, 73-113.
- [12] Esfahanian, V. 1991. Computation and stability analysis of laminar flow over a blunt cone in hypersonic flow, Ph.D. thesis, The Ohio State University.
- [13] Gaster, M. 1967. On the flow along swept leading edges, The Aeronautical Quarterly, Vol. XVIII, pp. 165-184.

- [14] Hall, P., Malik, M.R., Poll, D.I.A. 1984. On the stability of an infinitely swept attachment line boundary layer, Proc. R. Soc. Lond. A., 395:229-345.
- [15] Hall, P., Malik, M.R. 1986. On the instability of a three-dimensional attachment-line boundary layer: weakly nonlinear theory and a numerical approach, J. Fluid Mech., 163:257-282.
- [16] Haynes, T.S., Reed, H.L. 2000. Simulation of swept-wing vortices using nonlinear parabolized stability equations, Journal of Fluid Mechanics, 305, 325-349.
- [17] Högberg, M., Henningson, D. 1998. Secondary instability of crossflow vortices in Falkner–Skan–Cooke boundary layers. J. Fluid Mech. 368:339–57
- [18] Janke, E., Balakumar, P. 2000. On the secondary instability of three-dimensional boundary layers. Theoret. Comput. Fluid Dyn. 14:167–94
- [19] Joslin, R.D. 1995. Direct simulation of evolution and control of three-dimensional instabilities in attachment-line boundary layers, J. Fluid Mech., 291:369-392.
- [20] Joslin, R.D. 1996. Simulation of three-dimensional symmetric and asymmetric instabilities in attachment-line boundary layers, AIAA J., 34:2432-2434.
- [21] Kachanov, Y.S. 1996. Experimental studies 3-D instability boundary layer, AIAA 96-1976.
- [22] Kawakami M, Kohama Y, Okutsu M. 1999. Stability characteristics of stationary crossflow vortices in three-dimensional boundary layer. AIAA Pap. No. 99-0811
- [23] Kendall, J.M. 1975. Wind-tunnel experiments relating to supersonic and hypersonic boundary-layer transition. AIAA Journal, Vol. 13, No. 3, pp. 290-299.
- [24] Koch, W., Bertolotti, F.P., Stolte, A., Hein, S. 2000. Nonlinear equilibrium solutions in a 3-D boundary layer and their secondary instability. J. Fluid Mech. 406:131–74
- [25] Kohama, Y., Saric, W.S., Hoos, J.A. 1991. A high-frequency secondary instability of crossflow vortices that leads to transition, Proceedings of Boundary Layer Transition and Control Conference, Peterhouse College, Cambridge, United Kingdom, April.
- [26] Kohama, Y., Onodera, T., Egami, Y. 1996. Design and control of crossflow instability field. See Duck & Hall, pp. 147–56
- [27] Kufner, E., Dallmann, U., Stilla, J. 1993. Instability of hypersonic flow past blunt cones – effects of mean flow properties, AIAA Paper No. 93-2983.
- [28] Lerche, T. 1996. Experimental investigation of nonlinear wave interactions and secondary instability in three-dimensional boundary-layer flow. In 6th European Turbulence Conference, Lausanne (ed. S. Gavrilakis, L. Machiels, P.A. Monkewitz), pp. 357-60
- [29] Lin, R.S., Malik, M.R. 1996. On the stability of attachment-line boundary layers. Part 1. The incompressible swept Hiemenz flow. J. Fluid Mech., 311:239-255.
- [30] Lin, R.S., Malik, M.R. 1997. On the stability of attachment-line boundary layers. Part 2. The effect of leading edge curvature. J. Fluid Mech., 333:125-137.

- [31] Lyttle, I.J., Reed, H.L., Shipliyuk, A.N., Maslov, A.A., Buntin, D.A., Schneider, S.P. 2005. Numerical-experimental comparisons of second-mode behavior for blunted cones, *AIAA Journal*, Vol. 43, No. 8, 1734-43, Aug 2005.
- [32] Mack, L.M. 1984. Boundary-layer linear stability theory. Special Course on Stability and Transition of Laminar Flows, AGARD Report No. 709
- [33] Mack, L.M. 1987. Review of linear compressible stability theory. In *Stability of Time Dependent and Spatially Varying Flows*, ed. D.L. Dwoyer, M.Y. Hussaini, pp. 164-87. New York: Springer-Verlag.
- [34] Malik, M. R., Spall, R. E., Chang, C.-L. 1990. Effect of Nose Bluntness on Boundary Layer Stability and Transition. *AIAA Paper No. 90-0112*.
- [35] Malik, M.R., Li, F., Chang, C.L. 1994. Crossflow disturbances in three-dimensional boundary layers: nonlinear development, wave interaction and secondary instability, *Journal of Fluid Mechanics*, 268, 1-36.
- [36] Malik, M.R., Li, F., Chang, C.L. 1996. Nonlinear crossflow disturbances and secondary instabilities in swept-wing boundary layers. *IUTAM Symposium on Nonlinear Instability and Transition in Three-Dimensional Boundary Layers* (Duck P.W., Hall P., eds.), Amsterdam: Kluwer. 436pp.
- [37] Malik, M.R., Li, F., Choudhari, M., Chang, C. 1999. Secondary instability of crossflow vortices and swept-wing boundary layer transition. *J. Fluid Mech.* 399:85–115
- [38] Maslov, A. 2001. Experimental study of stability and transition of hypersonic boundary layer around blunted cone boundary layer around blunted cone,” *Tech. Rep. 1863-2000*, Institute of Theoretical and Applied Mechanics, December.
- [39] Morkovin, M.V. 1991. Panoramic view of changes in vorticity distribution in transition instabilities and turbulence, *Boundary Layer Stability and Transition to Turbulence*, FED-Vol. 114, editors D.C. Reda, H.L. Reed, and R. Kobayashi, ASME, New York, pp 1-16.
- [40] Pfenninger, W. 1965. Some results from the X-21 program. Part I. Flow phenomenon at the leading edge of swept wings. *AGARDograph No. 97*.
- [41] Pfenninger, W., Bacon, J.W. 1969. Amplified laminar boundary layer oscillations and transition at front attachment line of 45° swept flat-nosed wing with and without boundary layer suction, *Viscous Drag Reduction*, C Sinclair Wells, ed., Plenum Press, 85-105
- [42] Poll, D.I.A. 1979. Transition in the infinite swept attachment line boundary layer, *The Aeronautical Quarterly*, 30:607-629.
- [43] Poll, D.I.A. 1985. Some observations of the transition process on the windward face of a long yawed cylinder. *J. Fluid Mech.* 150:329-56
- [44] Radeztsky, R.H. Jr., Reibert, M.S., Saric, W.S., Takagi, S. 1993. Effect of micron-sized roughness on transition in swept-wing flows. *AIAA Paper 93-0076*.

- [45] Radeztsky, R.H. Jr., Reibert, M.S., Saric, W.S. 1994. Development of stationary crossflow vortices on a swept wing, AIAA Paper 94-2373.
- [46] Reed, H.L., Saric, W.S. 1989. Stability of three-dimensional boundary layer, Annual Review of Fluid Mechanics, Vol. 21, 1989, pp. 235-284.
- [47] Reed, H., Saric, W. 2008. Transition mechanisms for transport aircraft, AIAA-2008-3743.
- [48] Reibert, M.S., Saric, W.S., Carrillo, R.B., Chapman, K.L. 1996. Experiments in nonlinear saturation of stationary crossflow vortices. AIAA Paper 96-0184.
- [49] Rhodes, R.G., Carpenter, A.L., Reed, H.L., Saric, W.S. 2008. CFD analysis of flight-test configuration for LFC on swept wings. AIAA-2008-7336.
- [50] Rosenbloom, I., Hein, S., Dallmann, U. 1999. Influence of nose bluntness on boundary-layer instabilities in hypersonic cone flows, AIAA Paper No. 99-3591.
- [51] Rosenhead, L. (ed.), 1963. Laminar boundary layers, Oxford University Press.
- [52] Saric, W.S. 1994. Görtler Vortices, Annual Review of Fluid Mechanics, 26, 379-409.
- [53] Saric, W.S., Carrillo, R.B., and Reibert, M.S. (1998) "Leading-Edge Roughness as a Transition Control Mechanism," AIAA Paper 98-0781.
- [54] Saric, W.S., Reed, H.L., White, E.B. 2003. Stability of three-dimensional boundary layers, Annual Review of Fluid Mechanics, Volume 35, 2003.
- [55] Saric, W.S., Reed, H.L., Banks, D. 2004. Flight testing of laminar flow control in high-speed boundary layers," Saric, Reed, Banks, NATO-RTO-MP-AVT-111, Oct.
- [56] Saric, W.S., Carpenter, A.L., Reed, H.L. 2008. Laminar flow control flight tests for swept wings: strategies for LFC analysis, AIAA-2008-3834.
- [57] Schneider, S. P. 2001. Hypersonic laminar instability on round cones near zero angle of attack, AIAA Paper No. 01-0206.
- [58] Schneider, S. P., Matsumara, S., Rufner, S., Skoch, C., Swanson, E. 2002. Progress in the operation of the Boeing/AFOSR Mach-6 Quiet Tunnel, AIAA Paper No. 02-3033.
- [59] Spalart, P.R. 1989. DNS of leading-edge contamination. AGARD-CP No.438.
- [60] Stetson, K.F., Thompson, E.R., Donaldson, J.C., Siler L.G. 1984. Laminar boundary layer stability experiments on a cone at Mach 8, part 2: blunt cone. AIAA 84-0006.
- [61] Wasserman P, Kloker, M. 2002. Mechanisms and control of crossflow-vortex induced transition in a 3-D boundary layer. J. Fluid Mech. 456:49-84
- [62] White, E.B., Saric, W.S. 2005. Secondary instability of crossflow vortices. J. Fluid Mech. 525:275-308.